Strong antiferromagnetic spin fluctuations and the quantum spin-liquid state in geometrically frustrated β-Mn, and the transition to a spin-glass state caused by non-magnetic impurity

1997 J. Phys.: Condens. Matter 9 4701

(http://iopscience.iop.org/0953-8984/9/22/022)

J. Phys.: Condens. Matter **9** (1997) 4701–4728. Printed in the UK PII: S0953-8984(97)76489-0

Strong antiferromagnetic spin fluctuations and the quantum spin-liquid state in geometrically frustrated β-Mn, and the transition to a spin-glass state caused by non-magnetic impurity

H Nakamura†, K Yoshimoto†§, M Shiga†, M Nishi‡ and K Kakurai‡

† Department of Materials Science and Engineering, Kyoto University, Kyoto 606-01, Japan
‡ Neutron Scattering Laboratory, ISSP, The University of Tokyo, 106-1 Shirakata Tokai, Ibaraki 319-11, Japan

Received 19 July 1996, in final form 28 January 1997

Abstract. The magnetic properties of β-Mn and the effect of the substitution of non-magnetic Al were systematically investigated by measuring thermodynamic and transport properties, and the NMR and polarized neutron scattering for β-$Mn_{1-x}Al_x$ alloys with $0 \leqslant x \leqslant 0.4$. β-Mn is paramagnetic down to the lowest temperature (1.4 K) but with strong spin fluctuations. Substitution of Al atoms which preferentially occupy one of two crystallographic sites (site II) results in the formation of local moments on Mn atoms, and makes the ground state into a spin-glass-like state. NMR measurements revealed almost independent magnetic behaviour of the two different sites, and static magnetic ordering of Mn at site II for $x \geqslant 0.05$, although the possibility of very weak magnetism of the site-I atoms cannot be excluded. The temperature dependence of the spin–lattice relaxation rate $1/T_1$ indicates antiferromagnetic correlations of paramagnetic spin fluctuations, and its saturation at higher temperatures for β-$Mn_{0.97}Al_{0.03}$ and a critical slowing down of the fluctuations at low temperatures for β-$Mn_{0.9}Al_{0.1}$. Polarized neutron scattering experiments showed directly strong spin fluctuations with antiferromagnetic correlations for both β-Mn and β-$Mn_{0.9}Al_{0.1}$. The characteristic energy of fluctuations for β-Mn is fairly large even at 7 K ($2\Gamma = 40 \pm 10$ meV), implying a quantum origin of the fluctuations, while the energy spectrum of β-$Mn_{0.9}Al_{0.1}$ becomes very sharp at low temperatures, within a resolution-limited energy width, indicating damping of spin fluctuations into a spin-glass-like state. These results can be interpreted in terms of the transition from a spin liquid to a spin glass caused by the substitution of Al that gives rise to the release of the antiferromagnetic frustration of the characteristic crystal lattice. Considerable similarity of the characteristic features to those of the highly frustrated Laves phase compounds $Y(Sc)(Mn_{1-x}Al_x)_2$ is argued. The possible frustration on site II in the β-Mn structure, a three-dimensional network of corner-sharing regular triangles, which is similar to the two-dimensional Kagomé lattice, is pointed out.

1. Introduction

Manganese has four allotropies: the phases α, β, γ, and δ. The α-phase with the cubic A12 structure, which is the equilibrium phase at room temperature, is antiferromagnetic. The high-temperature phases γ and δ, which form fcc and bcc lattices, respectively, are hard to obtain at room temperature. β-Mn, which can easily be obtained by quenching, does not show any magnetic ordering down to the lowest temperature as was shown by

§ Present address: Materials and Devices Laboratory, Matsushita Electric Industrial Company Limited, Moriguchi, Osaka 570, Japan.

0953-8984/97/224701+28$19.50

neutron diffraction and NMR measurements [1, 2]. Due to the variation of the magnetism depending on the crystal structure, numerous studies of manganese metals have already been accumulated. Recent investigations revealed that, although β-Mn is paramagnetic down to the lowest temperature, it is characterized by large spin fluctuations as suggested by, for example, a large electronic specific heat coefficient γ [3], and a characteristic temperature dependence of the nuclear spin–lattice relaxation rate $1/T_1$ [4] which indicates antiferromagnetic correlations in spin fluctuations. One of the purposes of this study is to investigate the real nature of the magnetism in β-Mn, and the origin of the magnetically disordered ground state.

The concept of geometrical frustration of antiferromagnetic interactions was first recognized to be important for describing the magnetic properties of insulators, especially low-dimensional systems such as triangular and Kagomé lattices, and, later, extended to three-dimensional systems such as the fcc lattice and the corner-sharing tetrahedral lattice found in the pyrochlore and spinel structures (as recent reviews, see references [5–7]). Recently, however, it was revealed that effects of frustration are important even in metallic antiferromagnets, although we generally expect long-range magnetic interactions in such substances. For the manganese-based Laves phase itinerant magnets, RMn_2, the effects of frustration have been especially extensively investigated both experimentally [8] and theoretically [9–11]. A typical example is found in the cubic C15-type compound $Y(Sc)Mn_2$, which shows heavy-fermion-like behaviour. This compound exhibits the magnetically disordered ground state realized due to the frustration, suppressing strong antiferromagnetic correlations [12–22]. Effects of non-magnetic impurity on the magnetism of $Y(Sc)Mn_2$ were studied by preparing $Y(Sc)(Mn_{1-x}Al_x)_2$ compounds [19–22]. It was shown that the substitution of a small amount of Al for Mn results in the formation of Mn local moments and a spin-glass-like ground state. Giant spin fluctuations of quantum origin found in $Y(Sc)Mn_2$ were interpreted as being the result of frustration of the characteristic sublattice structure, i.e. a network of corner-sharing tetrahedra, where frustration of antiferromagnetic Heisenberg as well as Ising spins has already been discussed theoretically [23–26]. The evolution of the spin dynamics (the spin-liquid–spin-glass transition) in the $Y(Sc)(Mn_{1-x}Al_x)_2$ system was ascribed to the partial lifting of spin-configurational degeneracies due to the Al substitution. Recently, a heavy-fermion-like behaviour has been argued for theoretically in terms of the peculiar q-dependence of the spin-fluctuation spectrum originating in the strong geometrical frustration [11], which has actually been observed via neutron scattering measurements [18]. Since the physical properties of β-Mn are markedly similar to those of $Y(Sc)Mn_2$, it is of great interest to study the effect of Al substitution on the spin fluctuations in β-Mn. As will be shown, remarkable similarity was found for these systems. Hence, another purpose of this paper is to review detailed experimental results that show the evolution of the spin dynamics in the β-$Mn_{1-x}Al_x$ system, and to discuss its origin. In the 1970s, a number of studies of impurity effects on the magnetism of β-Mn were carried out, and 'weak' antiferromagnetic ordering was found in alloys [3, 4, 27–32]. The appearance of the magnetic ordering was explained as being a result of lattice expansion and/or the increase of the average number of d electrons. In the present study, however, we discuss the magnetic properties of β-Mn(Al) alloys from a different point of view but in the same context as for the $Y(Sc)(Mn_{1-x}Al_x)_2$ system, i.e. the frustration of antiferromagnetic interactions. The possibility of geometrical frustration on the β-Mn structure will also be discussed.

In this paper, we report systematic measurements of thermodynamic and transport properties, and the NMR and polarized neutron scattering of β-$Mn_{1-x}Al_x$ alloys with $0 \leqslant x \leqslant 0.4$. Noting the similarity to the $Y(Sc)(Mn_{1-x}Al_x)_2$ system [19], we point out that the ground state of β-Mn may be in a quantum spin-liquid state due to magnetic

frustration, and that the Al substitution causes a spin-liquid–spin-glass transition as a result of partial removal of spin-configurational degeneracies. In other words, the spin fluctuations in this system change from very dynamical (quantum) fluctuations to more static ones, keeping antiferromagnetic correlations. It is stressed that β-Mn is not a 'weak' magnet as was anticipated, but has a large dynamical moment, and that the magnetic ordering is suppressed by the geometrical frustration. Parts of the study have already been reported elsewhere [33–35].

2. Experimental procedures

Polycrystalline ingots (50–70 g) of Mn–Al alloys were prepared from 99.95% pure Mn and 99.99% pure Al in nominal concentrations by induction melting in an Ar atmosphere. After the melting, the solutes were kept for several minutes just above the melting point to homogenize the samples, and then cooled gradually to room temperature to avoid the introduction of strain. Since the β-phase of $Mn_{1-x}Al_x$ alloys with $x \leqslant 0.05$ is not the equilibrium phase at room temperature but the high-temperature phase, polycrystalline samples of β-$Mn_{1-x}Al_x$ with $x = 0, 0.03$ and 0.05 were obtained by rapid quenching of the high-temperature phase into iced water after annealing in evacuated quartz tubes at 900 °C for two days. A part of the ingot was crushed into fine powder for x-ray diffraction measurements. No foreign phase was detected for $x \leqslant 0.4$. As will be shown, two different crystallographic sites are present in the A13 structure. In order to determine the site occupied by Al atoms, a Rietveld refinement analysis was made for the powder x-ray diffraction pattern of β-$Mn_{0.8}Al_{0.2}$ measured via step scans.

The temperature dependence of the magnetic susceptibility was measured by using a torsion-type magnetic balance under an applied field of 8.23 kOe. The electrical resistivity was measured using a four-probe method. The thermal expansion was measured with a dilatometer of differential-transformer type. The specific heat was measured using an adiabatic method between 1.4 and 8 K.

For nuclear resonance measurements the samples were crushed into fine powder with the particle diameter less than 50 μm to avoid the skin-depth effect. Spin-echo NMR measurements including the nuclear quadrupole resonance (NQR) and antiferromagnetic nuclear resonance (AFNR) were made with a phase-coherent pulsed spectrometer. The nuclear spin–lattice relaxation time T_1 was measured for β-$Mn_{0.97}Al_{0.03}$ and β-$Mn_{0.9}Al_{0.1}$ alloys in the paramagnetic state by the conventional saturation–recovery method with saturation pulses. The gyromagnetic ratio for ^{55}Mn, $^{55}\gamma_n/2\pi = 1.050$ MHz kOe^{-1}, was used for analyses.

Neutron scattering was performed for pure β-Mn and alloyed β-$Mn_{0.9}Al_{0.1}$ by using about 60 g of coarse powder. In order to observe the magnetic scattering directly, polarized neutron scattering experiments were performed using the ISSP Polarized Neutron Triple Axis Spectrometer, PONTA-5G, installed at the reactor JRR-3M, in the Japan Atomic Energy Research Institute (JAERI). The (111) planes of magnetized Heusler alloys were used as the monochromator and analyser. Magnetic guide fields were used along the beam path to maintain the polarization of neutrons, and a flipping coil was placed between the monochromator and the sample. A weak magnetic field was applied at the sample position to orient the neutron polarization either along the direction of the scattering vector $\boldsymbol{Q}$ or perpendicular to $\boldsymbol{Q}$. Both constant-energy and constant-$\boldsymbol{Q}$ scans were carried out at 7 and 290 K for pure β-Mn and 7, 60, and 290 K for β-$Mn_{0.9}Al_{0.1}$. The fixed incident neutron energy was 80 meV for pure β-Mn and 34 meV for β-$Mn_{0.9}Al_{0.1}$. The collimations were chosen to be 40′–80′–80′–80′ and open (40′)–40′–40′–80′, respectively. The energy

resolution of the spectrometer was $2\Gamma_{res} = 19.3$ meV for the former and 5.8 meV for the latter conditions, as determined by vanadium incoherent elastic measurements. A $\boldsymbol{Q}$-scan for β-$Mn_{0.9}Al_{0.1}$ was also measured in the former conditions only at 290 K. In order to calibrate the intensities and to measure the intrinsic polarization of the instruments, the elastic scattering of the (221)/(300) nuclear Bragg peak was monitored under each set of conditions. The flipping ratios were 18–20 for all conditions. Raw count rates for vertical ($\boldsymbol{H} \perp \boldsymbol{Q}$) and horizontal ($\boldsymbol{H} \parallel \boldsymbol{Q}$) fields at the sample position, and for spin-flip (flipper on) and non-spin-flip (flipper off) conditions were corrected for finite polarization. Scattering in the spin-flip condition was accumulated for about 30 minutes in each field, and that in the non-spin-flip condition, which was used to correct the depolarization of neutrons, was counted for about five minutes in each field. The corrections were made by following the method described by Ziebeck and Brown [36]. The pure magnetic scattering was estimated by subtracting corrected spin-flip count rates for $\boldsymbol{H} \perp \boldsymbol{Q}$ from those for $\boldsymbol{H} \parallel \boldsymbol{Q}$. Magnetic intensities measured in inelastic conditions were corrected for the analyser transmission in the manner of Dorner [37].

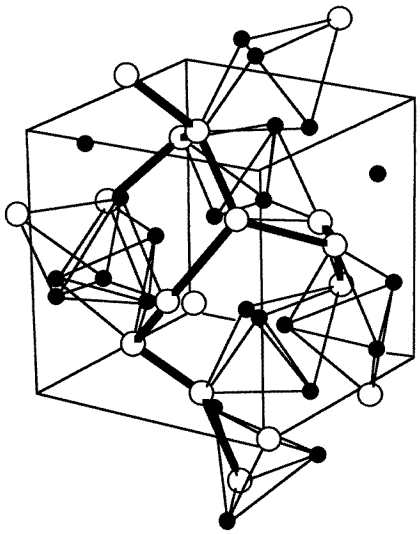

Figure 1. The crystal structure of β-Mn (cubic A13 type). The space group is $P4_132$. There are two inequivalent crystallographic sites. Open and solid circles represent site-I (8c-site) and site-II (12d-site) atoms, respectively. It should be noted that bonds are not necessarily drawn for nearest neighbours in this figure (see section 7.2).

3. Crystallography for β-Mn(Al)

β-Mn forms the cubic A13-type structure that contains 20 atoms in the unit cell [38]. The structure is shown schematically in figure 1. At a first sight, it looks very complicated. The space group is $P4_132$, which is characterized by the tetragonal screw axis 4_1. There are two inequivalent sites, which are usually called sites I (the 8c site) and II (the 12d site). The site symmetry is trigonal around the $\langle 111 \rangle$ axis and orthorhombic with the symmetry axis $\langle 110 \rangle$ for sites I and II, respectively.

Figure 2 shows the concentration dependence of the lattice parameter at room temperature. With increasing Al content, the lattice parameter increases rapidly at small

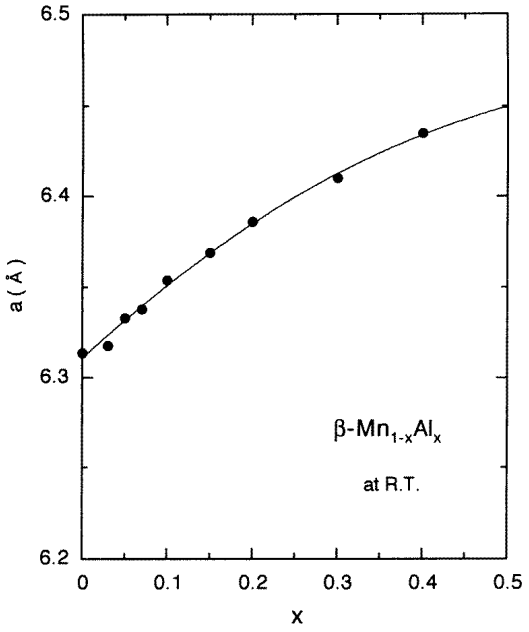

Figure 2. The concentration dependence of the lattice parameter at room temperature for β-$Mn_{1-x}Al_x$ alloys.

Al concentrations, and tends to saturate at larger Al concentrations. Similar behaviour was observed for the Y(Sc)$(Mn_{1-x}Al_x)_2$ system [19].

In order to determine the occupation ratio of Al atoms, the x-ray powder diffraction pattern for β-$Mn_{0.8}Al_{0.2}$ measured at room temperature was analysed using a Rietveld refinement program RIETAN [39]. It is very difficult to refine the occupation ratio and thermal vibration parameters independently, since they interact strongly with each other. Therefore, by fixing the occupation ratio to certain values, we looked for the optimal value for minimizing the R-factors and simultaneously giving reasonable thermal vibration parameters. The occupation ratios of Al thus obtained are 0.05 and 0.30 for sites I and II, respectively, indicating that about 90% of Al atoms locate at site II. It was reported that elements such as Fe, Co, and Ni with atomic radii smaller than that of Mn occupy site I, while those with larger radii, e.g. Sn, prefer site II [31, 40]. Our result is in accordance with this tendency.

4. Thermodynamic and transport properties

Figures 3(a) and 3(b) show the temperature dependence of the magnetic susceptibility χ of β-$Mn_{1-x}Al_x$ alloys ($0 \leqslant x \leqslant 0.4$). The susceptibility of pure β-Mn is almost constant against temperature. With increasing Al content, the magnitude of the susceptibility increases in spite of the fact that non-magnetic Al is substituted for Mn, and the temperature dependence approaches a Curie–Weiss-type one. For $x \geqslant 0.05$, a maximum was observed in the χ–T curve at a low temperature. The temperature of the maximum seems to increase with increasing Al content. For $x \geqslant 0.1$, the susceptibility in the high-temperature range is

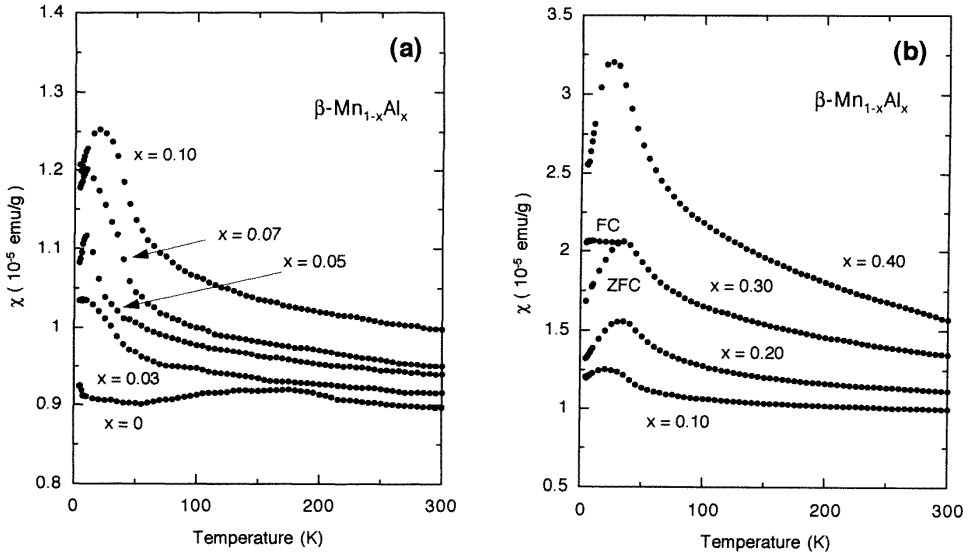

Figure 3. The temperature dependences of the magnetic susceptibilities for β-$Mn_{1-x}Al_x$ with $0 \leqslant x \leqslant 0.1$ (a) and with $0.1 \leqslant x \leqslant 0.4$ (b). The susceptibility measured for the zero-field-cooled sample is also shown for β-$Mn_{0.7}Al_{0.3}$.

well reproduced by the modified Curie–Weiss law

$$\chi = \chi_0 + \frac{C}{T - \theta} \tag{1}$$

where χ_0, C, and θ are constants. The concentration dependence of χ_0, θ, and μ_{eff} is shown in figure 4, where μ_{eff} is the effective paramagnetic moment deduced from C. The paramagnetic Curie temperatures θ are negative for all alloys, and the absolute value increases almost linearly with the Al concentration. With increasing Al content the effective moment μ_{eff} increases rapidly, while the temperature-independent susceptibility decreases monotonically. These results suggest that the substitution adds a localized-moment nature to the itinerant Mn 3d electrons. To check the origin of the maximum, the susceptibility was measured for the sample cooled in a field. The result for β-$Mn_{0.7}Al_{0.3}$ is shown in figure 3(b). The field-cooled sample shows temperature-independent susceptibility, suggesting a spin-glass-like freezing. Although the temperature of the maximum does not necessarily correspond to the spin-glass freezing point, T_f, its concentration dependence suggests that T_f increases gradually with increasing Al concentration and saturates at around $x = 0.3$.

Figure 5 shows the low-temperature specific heat C_L for β-$Mn_{1-x}Al_x$ alloys with $x = 0.05$, 0.1, and 0.2, where C_L/T was plotted against T^2. The scatter of the plots for $x = 0.05$ may be ascribed to poor thermal contact of the sample with the sample cell due to its large thermal expansion. For all samples, C_L/T is proportional to T^2 except in the low-temperature range. The electronic specific heat coefficient γ was estimated from the extrapolation of the high-temperature linear part. The concentration dependence of γ is shown in figure 6 together with the value for pure β-Mn reported by Shinkoda *et al* [3]. The extraordinarily enhanced γ for pure β-Mn is rapidly reduced by the substitution of Al, and is asymptotic to a normal value for usual metals at high Al concentrations, i.e. in the spin-glass region. According to a band calculation of β-Mn [41], the bare density of states at the Fermi level yields approximately $\gamma = 8$ mJ K^{-2} mol^{-1}, indicating an enhancement

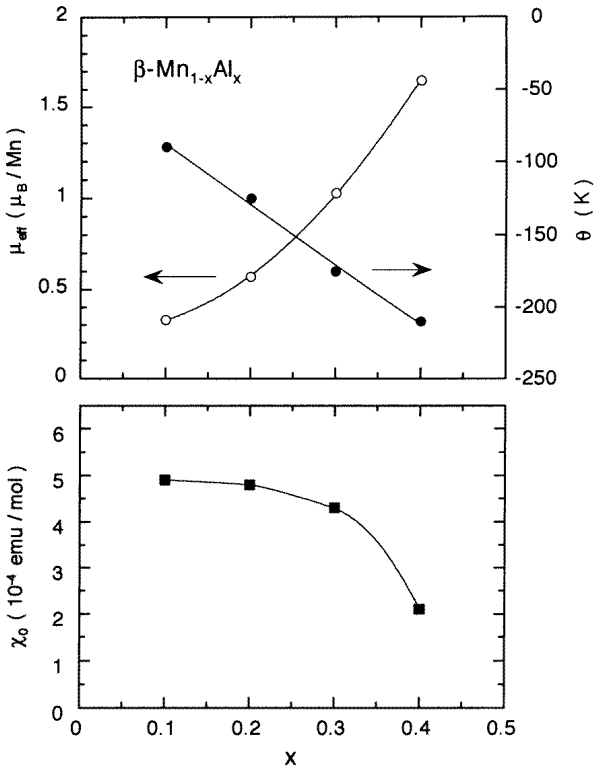

Figure 4. The concentration dependence of the effective paramagnetic moment (open circles), paramagnetic Curie temperature (solid circles), and temperature-independent susceptibility (squares) for β-$Mn_{1-x}Al_x$ alloys estimated from the susceptibility assuming equation (1).

of γ in β-Mn of one order of magnitude.

Figure 7 shows thermal expansion curves for β-$Mn_{1-x}Al_x$ alloys with $0 \leqslant x \leqslant 0.3$. For pure β-Mn the unit-cell volume increases rapidly with increasing temperature, while for $x \geqslant 0.03$ it exhibits temperature-independent behaviour at low temperatures, which corresponds to the spontaneous volume magnetostriction. The temperature range of the flat part increases with increasing Al concentration. The thermal expansion coefficient at around room temperature, which is markedly large for pure β-Mn ($\sim 30 \times 10^{-6}$ K^{-1}), decreases monotonically with increasing Al concentration and shows a fairly normal value for $x = 0.3$ ($\sim 15 \times 10^{-6}$ K^{-1}).

The temperature dependence of the electrical resistivity also changes remarkably upon the substitution of Al as shown in figure 8, where relative values normalized at 290 K are shown. The absolute values are somewhat large (150–250 $\mu\Omega$ cm), probably due to defects and/or microcracks in the samples introduced during the sample preparation. For pure β-Mn, the resistivity increases rapidly in proportion to T^2 at low temperatures, and tends to saturate at high temperatures. This result is in agreement with that in a previous report [42], and similar to the behaviour observed for the Y(Sc)Mn_2 system [19] and YMn_2 under pressure [43]. With increasing Al concentration, the resistivity becomes less sensitive to temperature, and exhibits a minimum for $x \geqslant 0.05$. The temperature of the minimum increases with increasing Al content, and only negative temperature coefficients were observed for $x \geqslant 0.2$

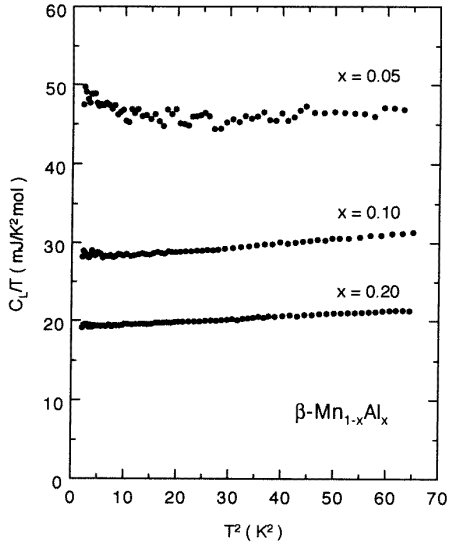

Figure 5. The low-temperature specific heat C_L for β-$Mn_{1-x}Al_x$ alloys with $x = 0.05$, 0.1, and 0.2, where C_L/T is plotted against T^2.

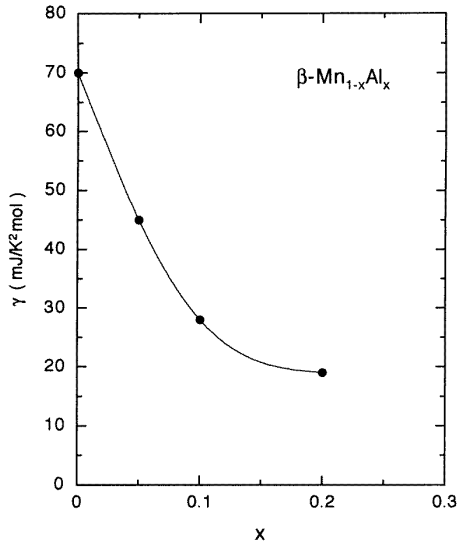

Figure 6. The concentration dependence of the electronic specific heat coefficient γ for β-$Mn_{1-x}Al_x$. The data for pure β-Mn were taken from reference [3].

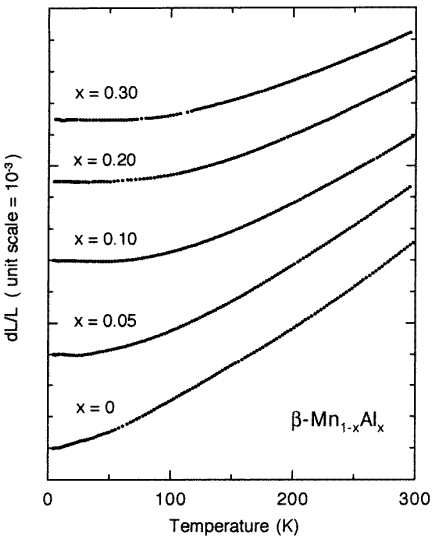

Figure 7. Thermal expansion curves for β-$Mn_{1-x}Al_x$ alloys.

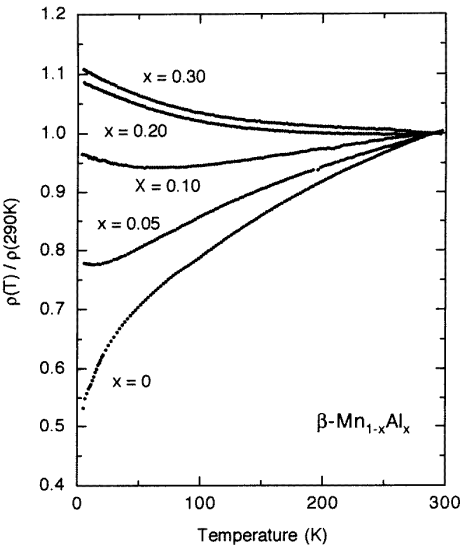

Figure 8. The temperature dependence of the electrical resistivity for β-$Mn_{1-x}Al_x$ alloys, which is normalized at 290 K.

below room temperature.

It is notable that Y(Sc)Mn_2 shows almost the same behaviour of the susceptibility, specific heat, thermal expansion, and electrical resistivity, suggesting that the electronic states of β-Mn and Y(Sc)Mn_2 systems are quite similar to each other. The markedly similar

effects of the Al substitution on these properties have also been found in the $Y(Sc)Mn_2$ system [19], indicating that the evolution of Mn magnetism induced by the Al substitution should be explained in the same context.

5. Nuclear magnetic resonance

5.1. Site assignment

As was already described in section 3, there are two inequivalent crystallographic sites in the β-Mn (A13) structure. An electric field gradient (EFG) exists at both sites due to the low site symmetry. It should be noted that the EFG at site I is axial, while that at site II is non-axial. At an early stage, Drain [44] had observed ^{55}Mn NMR from only one of the sites. The NMR signal was affected by a small quadrupole interaction with axial symmetry ($\nu_Q \sim 0.26$ MHz at 295 K). The author interpreted this as showing that the resonance arises from site I, taking account of the axial symmetry of the EFG and the small quadrupole interaction expected from point-charge calculations where EFG arising from nearest-neighbour atoms only were considered. Recently Kohori *et al* [45] found ^{55}Mn NMR and NQR from the other site, with a larger ν_Q of about 4.5 MHz and $\eta = 0$–0.1. They assigned this resonance to site II, following the discussion by Drain.

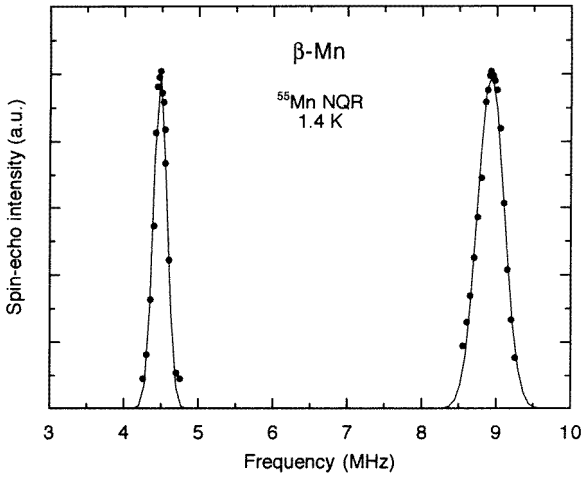

Figure 9. The ^{55}Mn NQR spectrum for β-Mn measured at 1.4 K. Solid lines are Gaussian functions fitted to experimental points. This resonance is assigned to site II (see the text).

We have also measured the NQR spectrum from the site with the larger ν_Q in β-Mn at 1.4 K. The result is shown in figure 9. Two lines corresponding approximately to transitions of $m = \pm 1/2 \leftrightarrow \pm 3/2$ and $m = \pm 3/2 \leftrightarrow \pm 5/2$ were observed at around 4.5 and 9 MHz, respectively. In the figure the signal intensities of the two lines are normalized, since the intensity ratio is not known due to the different experimental conditions. Both lines are well reproduced by Gaussian functions. The central frequencies and the full widths at half-maximum were estimated at $\nu_1 = 4.483 \pm 0.0033$ MHz, $\Delta\nu_1 = 0.215 \pm 0.009$ MHz, and $\nu_2 = 8.926 \pm 0.0046$ MHz, $\Delta\nu_2 = 0.420 \pm 0.011$ MHz for low- and high-frequency signals, respectively. It is notable that the linewidth of the high-frequency signal is approximately twice as large as that of the low-frequency signal. For the nuclear spin $I = 5/2$ and in the

case of sufficiently small η, the NQR lines are observed at

$$\nu_1 = \nu_Q\left(1 + \frac{59}{54}\eta^2\right) \qquad \nu_2 = 2\nu_Q\left(1 - \frac{11}{54}\eta^2\right) \tag{2}$$

where

$$\nu_Q = \frac{3e^2qQ}{2hI(2I-1)} \tag{3}$$

is the quadrupole frequency [46]. On using equation (2), the experimentally obtained resonance frequencies give $\nu_Q = 4.466 \pm 0.008$ MHz and $\eta = 0.059 \pm 0.009$. The non-zero η proves that the NQR signal comes from the site with non-axial local symmetry, i.e. site II, which is in agreement with the conclusion reached by Kohori *et al* [45]. We have not found any contradiction to this site assignment in other experimental results, as will be shown.

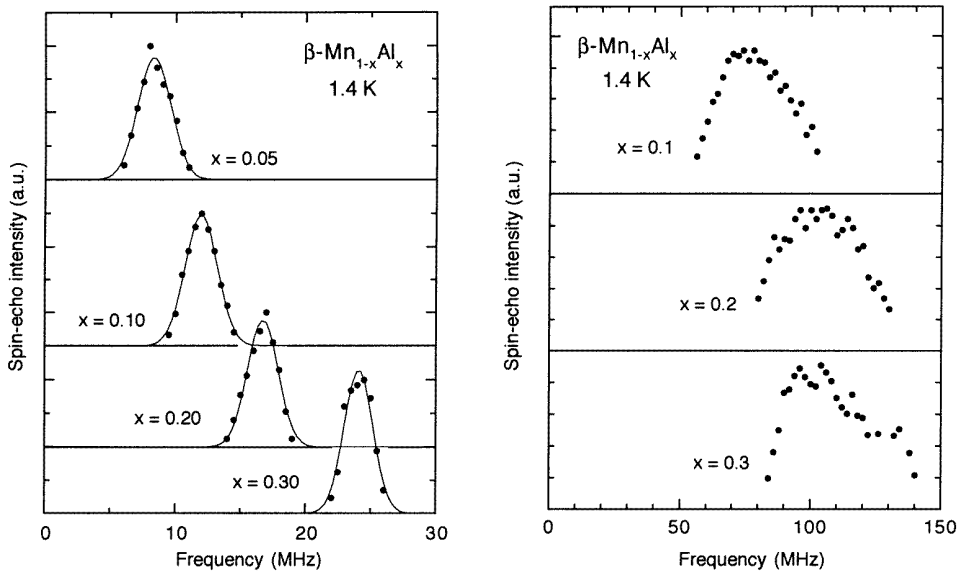

Figure 10. ^{55}Mn zero-field antiferromagnetic nuclear resonances observed in low-frequency (a) and high-frequency (b) ranges at 1.4 K for β-$Mn_{1-x}Al_x$ alloys with $x \geqslant 0.05$. The solid lines in (a) are Gaussian functions fitted to experimental points. For $x = 0.05$, although a weak resonance was observed at around 50 MHz, the signal-to-noise ratio is too poor for measuring the whole spectrum.

5.2. Ground-state properties

The ground states of β-$Mn_{1-x}Al_x$ alloys were investigated by performing field-swept and zero-field measurements at 4.2 and 1.4 K. For $x \leqslant 0.03$, we observed both the site-I ^{55}Mn NMR signal in field-swept measurements at a relatively low frequency, and the site-II ^{55}Mn NQR signal in zero-field measurements, indicating non-magnetic ground states for $x \leqslant 0.03$. It seems that the intensity of the NQR signal decreases markedly on the substitution of a small amount of Al, while that of the NMR signal is less sensitive to the substitution. This is consistent with the fact that Al atoms preferentially occupy site II. On the other hand,

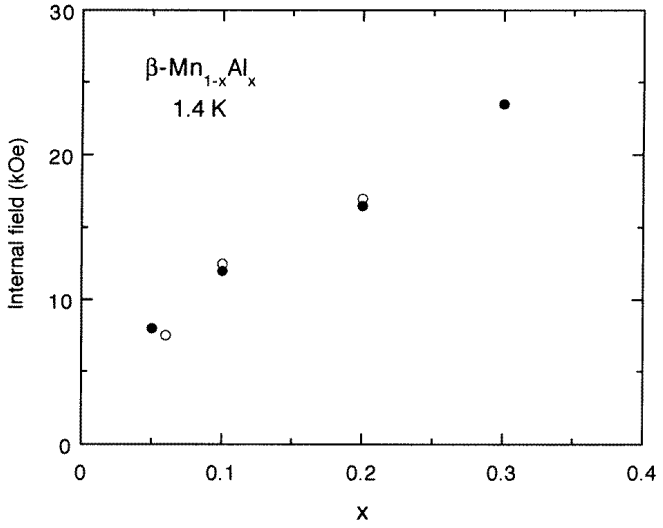

Figure 11. The concentration dependence of the internal field for β-$Mn_{1-x}Al_x$ alloys with $x \geqslant 0.05$ estimated from the low-frequency resonances in figure 10(a) (solid circles). The results reported by Katayama and Asayama [32] are also shown (open circles).

for $x \geqslant 0.05$, the ^{55}Mn NMR signal, which is observable at high temperatures, disappears at 4.2 K. The ^{55}Mn NQR signal could not be observed either at 4.2 K. Instead, different resonances were observed in zero field. Figures 10(a) and 10(b) show zero-field spectra observed for $x \geqslant 0.05$. Two different resonances were observed in low- and high-frequency ranges for each sample. The characters of these resonances are completely different. The linewidths of the low-frequency signals are much narrower than those of the high-frequency ones, and less sensitive to the amount of Al substitution. Figure 11 shows the resonance frequencies plotted against the Al concentration, which agree well with those reported previously by Katayama and Asayama [32]. The widths of the high-frequency resonances are markedly large: several tens of MHz. The high-frequency signals were observable only at lower temperatures (say, observable at 1.4 K but hard to observe at 4.2 K) presumably due to the strong temperature dependence of the nuclear relaxation time. The presence of these zero-field resonances indicates the appearance of the static magnetic ordering for $x \geqslant 0.05$, which is consistent with the spin-glass-like freezing suggested on the basis of the magnetic susceptibility. Two different zero-field signals indicate the presence of two different magnetic sites at low temperatures. Kohori *et al* [45] claimed that Mn atoms at site II are more strongly magnetic than those at site I since the nuclear spin–lattice relaxation rate $1/T_1$ is markedly different, i.e. $1/T_1$ at site II is about 20 times larger than that at site I. Therefore, it is reasonably considered that only Mn atoms at site II order magnetically at low temperatures, and that atoms at site I remain paramagnetic. That is, the lower-frequency signal can be assigned to site I which 'feels' only the transferred hyperfine field from site II. The narrow linewidth is consistent with a small quadrupolar effect of site I as was shown from paramagnetic resonances. On the other hand, the high-frequency signal arises from the magnetic site II frozen in a spin-glass-like state, whose nuclei 'feel' a large intra-atomic hyperfine field. It is notable that the signal appears at around 100 MHz, which corresponds to the internal field ~100 kOe, indicating a large static moment of the order of 1 μ_B (see section 7.1 and figure 20, later). We cannot deny the possibility that site I carries a small

ordered moment, but can state confidently that it must be negligible compared with the site-II moment.

Thus NMR studies revealed no magnetic ordering for $x \leqslant 0.03$, and an appearance of static magnetic ordering for $x \geqslant 0.05$. It should be emphasized that the magnetism at site I behaves almost independently of that at site II.

5.3. Nuclear spin–lattice relaxation in the paramagnetic state

The aim of the relaxation measurements is to investigate the evolution of the spin dynamics in the paramagnetic state caused by the substitution of Al. We hoped to measure $1/T_1$ directly for the magnetic site II using the NQR signal. It was, however, difficult to observe the NQR resonance for $x \geqslant 0.05$ over a wide temperature range due to poor signal-to-noise ratios. Therefore, we measured $1/T_1$ for site I using the ^{55}Mn NMR signal at a relatively low frequency (i.e. low fields). This is considered to give rather indirect information on the spin dynamics of the magnetic site II. We measured $1/T_1$ for β-$Mn_{0.97}Al_{0.03}$ and β-$Mn_{0.9}Al_{0.1}$; the former is paramagnetic down to the lowest temperature and the latter exhibits spin-glass-like freezing. (The results for pure β-Mn have already been published for both sites I [4] and II [45].)

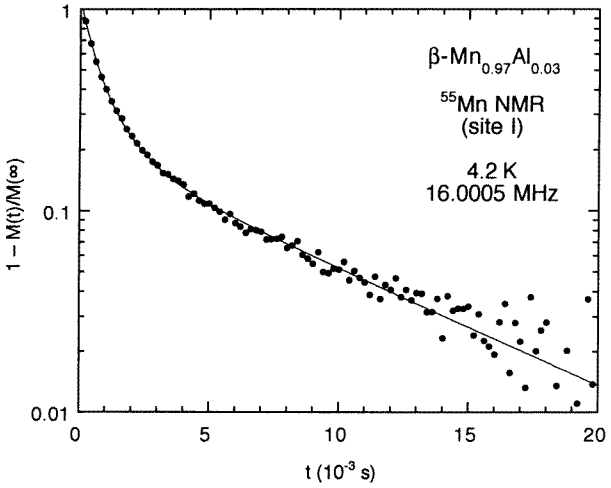

Figure 12. An example of the recovery curve of the nuclear magnetization measured for ^{55}Mn NMR (site I) for β-$Mn_{0.97}Al_{0.03}$ at 4.2 K and 16.0005 MHz. The solid curve represents equation (4) fitted to experimental points.

A typical example of the nuclear magnetization recovery is shown for β-$Mn_{0.97}Al_{0.03}$ in figure 12 on a semi-logarithmic scale. The curve is convex downwards, indicating a relaxation of multiple-exponential type. Although the origin of this multiple-exponential behaviour is not obvious, recognizing it as being due to the quadrupole interaction, we tried to fit the experimental data to the recovery function for $I = 5/2$ as follows:

$$M(t) = M(\infty)\left[1 - \left\{a_1 \exp\left(-\frac{t}{T_1}\right) + a_2 \exp\left(-\frac{6t}{T_1}\right) + a_3 \exp\left(-\frac{15t}{T_1}\right)\right\}\right] \tag{4}$$

where $M(t)$ is the spin-echo intensity as a function of time t after the saturation of the nuclear magnetization, and a_1, a_2, and a_3 are constants depending on the initial saturation

condition of the nuclear magnetization [47]. The three-exponential relaxation function simply originates in shifts of the nuclear ($I = 5/2$) Zeeman splittings caused by the quadrupole interaction. In this analysis we treated a_1, a_2, and a_3 as free parameters. This fitting procedure reproduces well the experimental recovery, as shown by the solid curve in figure 12.

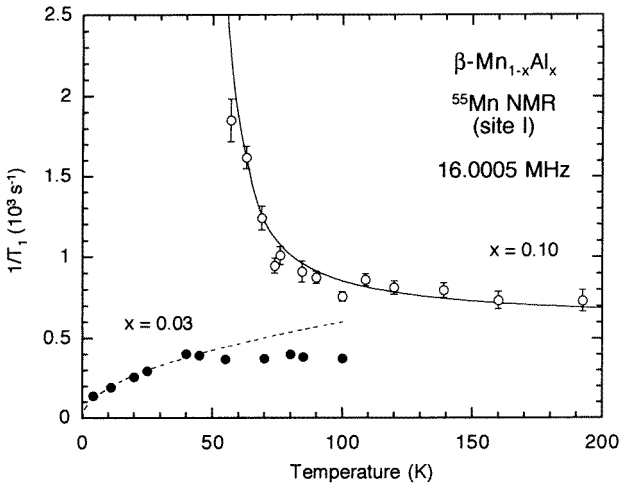

Figure 13. The temperature dependence of the nuclear spin–lattice relaxation rate $1/T_1$ measured for ^{55}Mn NMR (site I) for β-$Mn_{0.97}Al_{0.03}$ (solid circles) and β-$Mn_{0.9}Al_{0.1}$ (open circles). The broken curve indicates $\sqrt{T}$-dependence. The solid curve is $1/T_1$ (s^{-1}) $= 1.34 \times 10^4/(T - 47) + 600$, fitted to experimental points.

Figure 13 shows the temperature dependence of the spin–lattice relaxation rate $1/T_1$ thus obtained for β-$Mn_{0.97}Al_{0.03}$ and β-$Mn_{0.9}Al_{0.1}$. The results are contrasting. For β-$Mn_{0.97}Al_{0.03}$, $1/T_1$ increases with increasing temperature. The broken curve in the figure shows a tentatively drawn $\sqrt{T}$-dependence: $1/T_1 = 60\sqrt{T}$ s^{-1}. Thus, $1/T_1$ is roughly proportional to $\sqrt{T}$ at low temperatures, and shows a trend towards saturation above 50 K. For β-$Mn_{0.9}Al_{0.1}$, on the other hand, $1/T_1$ increases with decreasing temperature and shows a trend towards divergence at around 50 K. A tentative fit to the equation $1/T_1 = a/(T-b)+c$ reproduces the experimental data well with $a = 1.34\times10^4$ s^{-1} K^{-1}, $b = 47$ K, and $c = 600$ s^{-1}, as shown by the solid curve in figure 13. Similar behaviour has been observed for the Y(Sc)$(Mn_{1-x}Al_x)_2$ system [21]. The contrasting behaviour of the relaxation rate can be understood in terms of a spin-liquid–spin-glass transition caused by the Al substitution.

6. Neutron scattering

To see the spin fluctuations directly, we performed polarized neutron scattering experiments on a typical specimen, pure β-Mn, and alloyed β-$Mn_{0.9}Al_{0.1}$; the latter shows spin-glass-like ordering at low temperatures.

Figure 14 shows polarized $\boldsymbol{Q}$-scan spectra of β-Mn measured for energy transfer zero at 7 and 290 K. The intensity should be proportional to the integral of the squared amplitude of the spin fluctuations within the energy resolution of $2\Gamma_{res} = 19.3$ meV. A broad peak was observed at around $Q = 1.6$ Å^{-1}. This roughly corresponds to twice the mean interatomic

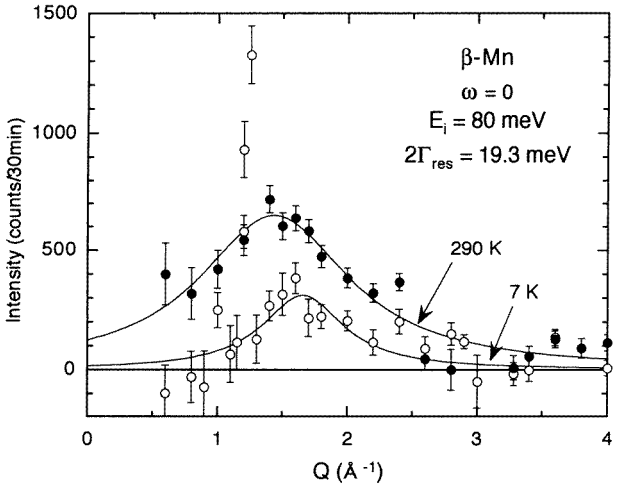

Figure 14. The magnetic neutron scattering rate of pure β-Mn as a function of the scattering vector Q measured at energy transfer zero with energy resolution $2\Gamma_{res} = 19.3$ meV at 7 K (open circles) and 290 K (solid circles). The solid curves are guides for the eyes. A sharp line observed at 7 K at around $Q = 1.2$ Å^{-1} can be ascribed to the (1/2 1/2 1/2) magnetic Bragg peak of antiferromagnetic MnO impurity (see the text).

distance, indicating antiferromagnetic correlations of spin fluctuations. The amplitude decreases with decreasing temperature. It should be noted, however, that scattering is still observable even at 7 K, suggesting the existence of strong zero-point spin fluctuations, as discussed later. A sharp peak at $Q = 1.2$ Å^{-1} in the spectrum at 7 K can be ascribed to the $(\frac{1}{2}\frac{1}{2}\frac{1}{2})$ magnetic peak arising from antiferromagnetic MnO impurity, possibly introduced by the sample oxidation during the experiments, since the intensity was found to be large several months after the initial experiment.

Figure 15 shows energy scan spectra of β-Mn measured at the wave vector $Q = 1.6$ Å^{-1} which is the peak position of the $\boldsymbol{Q}$-scan spectra for energy transfer zero. Generally the scattering function $S(\boldsymbol{q}, \omega)$ obtained from neutron scattering experiments can be related to the imaginary part of the dynamical susceptibility $\chi(\boldsymbol{q}, \omega)$ as follows:

$$S(\boldsymbol{q}, \omega) = \frac{\hbar}{\pi g^2 \mu_B^2} \frac{1}{1 - \exp(-\hbar\omega/k_B T)} \chi''(\boldsymbol{q}, \omega). \tag{5}$$

Usually a Lorentzian-type function is assumed for the energy dependence of the dynamical susceptibility:

$$\chi''(\boldsymbol{q}, \omega) = \chi(\boldsymbol{q}) \frac{\omega\Gamma}{\Gamma^2 + \omega^2} \tag{6}$$

where Γ is the characteristic energy of spin fluctuations, and $\chi(\boldsymbol{q})$ is the q-dependent static susceptibility. In experiments, due to the finite energy resolution of the spectrometer, the observed scattering is convoluted with the energy resolution function. For a crude analysis, assuming a simple Gaussian resolution function $R(\omega)$, the experimental spectra were fitted

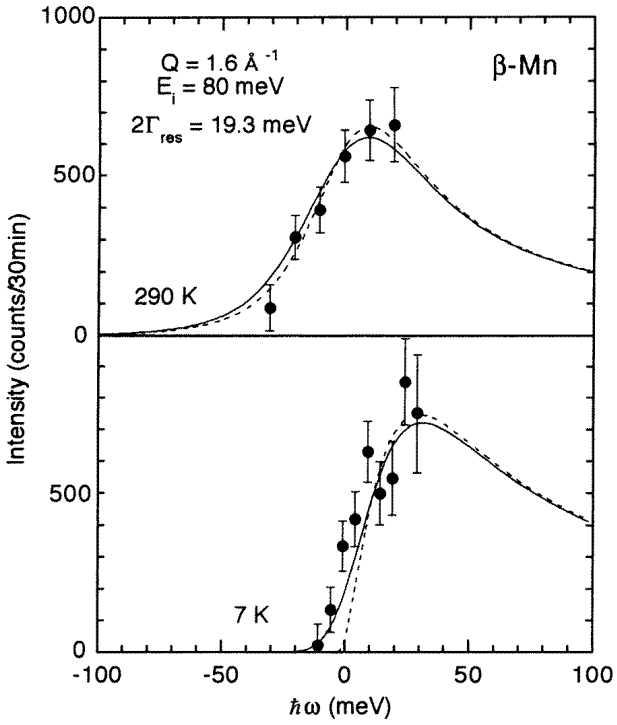

Figure 15. The magnetic neutron scattering rate of pure β-Mn as a function of the energy transfer $\hbar\omega$ measured at momentum transfer $Q = 1.6$ Å^{-1} with energy resolution $2\Gamma_{res} = 19.3$ meV at 7 and 290 K. The solid curves indicate spectra calculated assuming equations (5)–(7). The broken curves indicate deconvoluted spectra, i.e. $S(\boldsymbol{q}, \omega)$.

to

$$I(\boldsymbol{q}, \omega) = I_0 \int_{-\infty}^{+\infty} R(\omega - \omega') S(\boldsymbol{q}, \omega)\ \mathrm{d}\omega'$$
$$R(\omega) = \frac{1}{\Gamma_{res}} \sqrt{\frac{\ln 2}{\pi}} \exp\left(-\ln 2 \frac{\omega^2}{\Gamma_{res}^2}\right) \tag{7}$$

where I_0 is a constant depending on the experimental conditions. By choosing appropriate values of $\chi(\boldsymbol{q})$ and Γ, we obtained fairly good fits, as shown by the solid curves in figure 15. The dashed lines in the figure indicate the deconvoluted spectra, i.e. $S(\boldsymbol{q}, \omega)$. At 7 K, scattering was observable only on the neutron energy-loss side ($\omega > 0$). Since the energy spectral width is much larger than the thermal energy of 7 K ($\approx$0.6 meV) and remains finite at 0 K as seen in figure 16, we may regard the magnetic scattering at 7 K as zero-point spin fluctuations.

Figure 17 shows $\boldsymbol{Q}$-scan spectra measured for energy transfer zero for β-$Mn_{0.9}Al_{0.1}$ at 7, 60, and 290 K. A narrower energy resolution of the spectrometer, $2\Gamma_{res} = 5.8$ meV, was chosen for β-$Mn_{0.9}Al_{0.1}$. The spectral profiles are similar to those for pure β-Mn, having a broad peak at around $Q = 1.6$ Å^{-1}. This indicates antiferromagnetic correlations between Mn spins. In contrast to that of pure β-Mn, the scattering intensity increases with decreasing temperature. Figure 18 shows the energy spectra for β-$Mn_{0.9}Al_{0.1}$ measured at

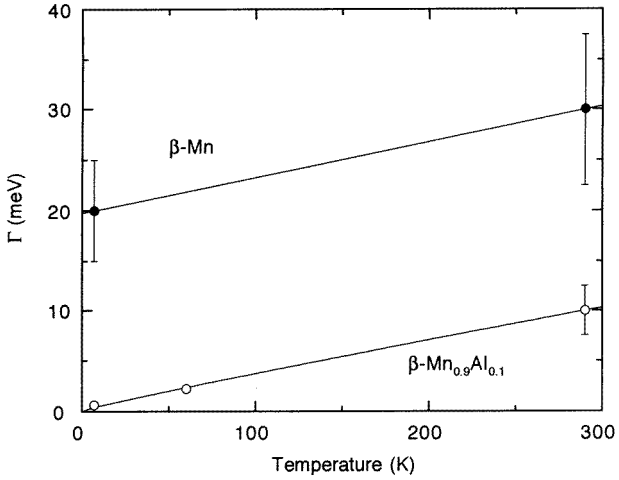

Figure 16. The temperature dependence of the quasi-elastic spectral width Γ for pure β-Mn (solid circles) and β-$Mn_{0.9}Al_{0.1}$ (open circles). The straight lines are guides for the eyes.

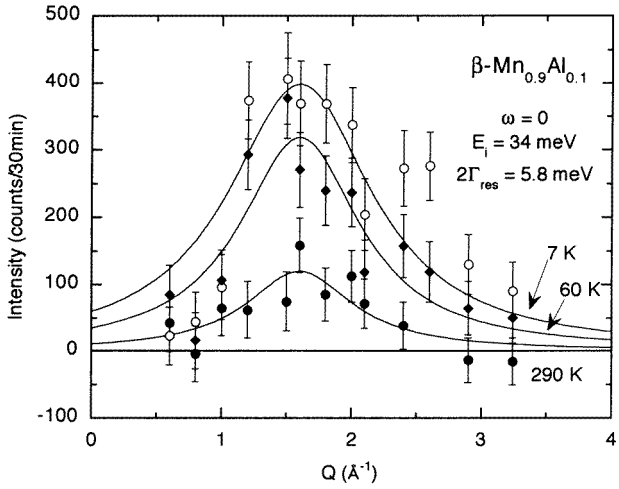

Figure 17. The magnetic neutron scattering rate of β-$Mn_{0.9}Al_{0.1}$ as a function of the scattering vector Q measured at energy transfer zero with energy resolution $2\Gamma_{res} = 5.8$ meV at 7 K (open circles), 60 K (squares), and 290 K (solid circles). The solid curves are guides for the eyes.

$Q = 1.6$ Å^{-1}. The energy dependence of the magnetic scattering is markedly different from that of pure β-Mn. The widths of the scattering function Γ, which are shown in figure 16, are much narrower than those of pure β-Mn, particularly at low temperatures, and approach zero at 0 K. These observations indicate that the spin fluctuations in β-$Mn_{0.9}Al_{0.1}$ become nearly static at low temperatures in accordance with the appearance of the static hyperfine field (observed in NMR experiments). Accordingly, we have also observed diffuse scattering in usual diffraction measurements at low temperatures. Similar diffuse scattering for β-Mn(Co) and β-Mn(In) alloys has been observed [48].

In order to compare the scattering intensities of pure β-Mn and β-$Mn_{0.9}Al_{0.1}$, we

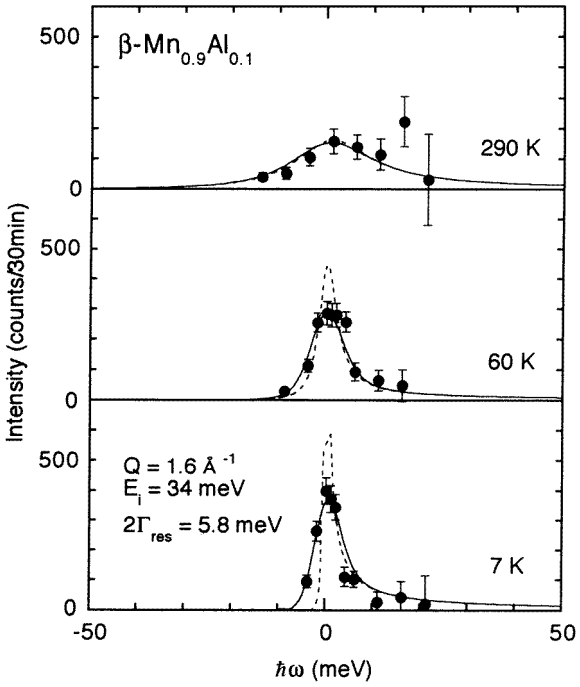

Figure 18. The magnetic neutron scattering rates for β-$Mn_{0.9}Al_{0.1}$ as functions of the energy transfer $\hbar\omega$ measured at momentum transfer $Q = 1.6$ Å^{-1} with energy resolution $2\Gamma_{res} = 5.8$ meV at 7, 60, and 290 K. The solid curves indicate spectra calculated assuming equations (5)–(7). The broken curves indicate deconvoluted spectra, i.e. $S(\boldsymbol{q}, \omega)$.

measured a $\boldsymbol{Q}$-scan spectrum of β-$Mn_{0.9}Al_{0.1}$ at 290 K in the same condition of the spectrometer as for taking the β-Mn spectrum, i.e. $2\Gamma_{res} = 19.3$ meV. The result is shown in figure 19. It is notable that the scattering intensity is comparable to that for β-Mn, as discussed in detail below.

7. Discussion

7.1. Spin fluctuations in β-Mn(Al)

Our NMR experiments have shown that the magnetism of sites I and II can be recognized as independent in the ordered states for Al-substituted alloys. Even if site II exhibits spin-glass-like freezing, site I remains non-magnetic (or weakly magnetic). The relaxation rates measured for each site in pure β-Mn [4, 45] demonstrated that site II exhibits stronger antiferromagnetic spin fluctuations in the paramagnetic state. Thus site II is more magnetic, and is responsible for the characteristic magnetic properties of the β-$Mn_{1-x}Al_x$ system. This fact was also suggested by a Knight shift analysis for a high-temperature range [49]. Although why only site II is magnetic is not explicit, this fact suggests that the 3d electron levels of site-I atoms are far below the Fermi level and/or the site-I contribution to the Fermi level density of states is small, which is consistent with a crystallographic character; site I is more compact than site II in the sense that the nearest-neighbour distance between site-I atoms is smaller than that between site-II atoms. It should be noticed that such

different magnetic properties depending on crystallographic sites have already been found for antiferromagnetic α-Mn, in which each site has its own magnitude of the ordered moment [50]. Here, we try to estimate approximate values of the ordered moment at site II in the alloys with $x \geqslant 0.05$. For this purpose we assume the same hyperfine coupling mechanism for α- and β-Mn. The hyperfine coupling has already been given for antiferromagnetic α-Mn [51] in which four crystallographic Mn sites exhibit different moment values, and hence different hyperfine fields ranging over 20–100 kOe/μ_B (see figure 2 in reference [51]). Assuming continuous variation of the hyperfine coupling constant against the moment value, crude values of the ordered moment were estimated from the zero-field NMR frequencies (figure 10(b)) as shown in figure 20. The moment values are fairly large—of the order of 1 μ_B.

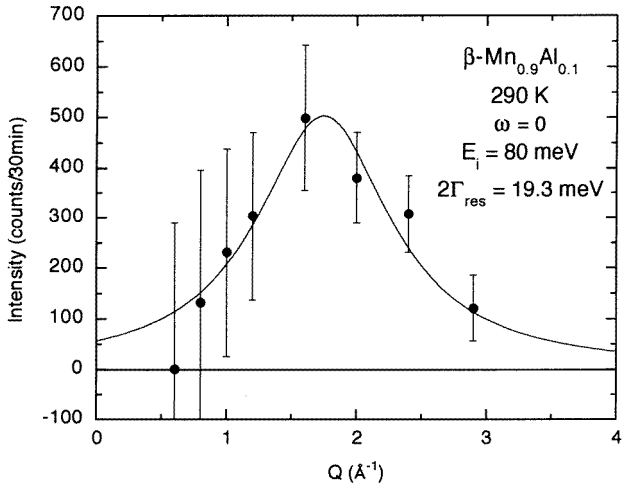

Figure 19. The magnetic neutron scattering rate of β-$Mn_{0.9}Al_{0.1}$ as a function of the scattering vector Q measured at energy transfer zero with energy resolution $2\Gamma_{res} = 19.3$ meV at 290 K. The solid curves are guides for the eyes.

Next we discuss the spin fluctuations observed via neutron scattering measurements. For pure β-Mn, we observed strong paramagnetic scattering centred at $Q \sim 1.6$ Å^{-1} at both high and low temperatures. This result directly proves the existence of strong spin fluctuations with antiferromagnetic correlations in β-Mn, indicating that β-Mn is not a conventional Pauli paramagnet, but is one of the strongly correlated electron systems. The large spin fluctuations observed at 7 K cannot be ascribed to thermal fluctuations, but can be ascribed to a quantum origin that will be called zero-point fluctuations. The definition of zero-point fluctuations is rather controversial but, here, following the discussion given by Takahashi [52, 53], we use a rather extended definition, i.e. the difference between total dynamical fluctuations and thermal fluctuations which can exist not only at 0 K, but also at any other temperature. Then we divide the squared local spin-fluctuation amplitude $\langle S_L^2 \rangle$ into three components, as follows:

$$\langle S_L^2 \rangle = \langle S_L^2 \rangle_{ZP} + \langle S_L^2 \rangle_{TH} + \langle S_L^2 \rangle_{ST} \tag{8}$$

where $\langle S_L^2 \rangle_{ZP}$ is the average squared amplitude of zero-point spin fluctuations, $\langle S_L^2 \rangle_{TH}$ is that of thermal spin fluctuations, and $\langle S_L^2 \rangle_{ST}$ is that of the static local spin induced by molecular fields. Since the thermal fluctuations $\langle S_L^2 \rangle_{TH}$ should be zero at 0 K, the

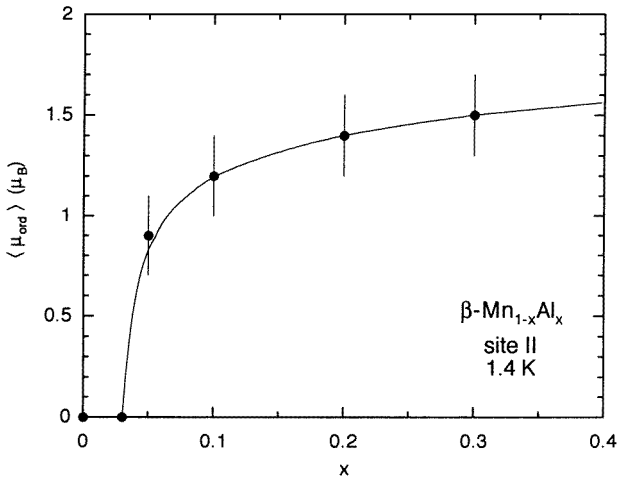

Figure 20. A rough estimation of the average values of the ordered moment per Mn atom in site II for β-$Mn_{1-x}Al_x$, based on the hyperfine field, assuming the same hyperfine coupling as for antiferromagnetic α-Mn (see the text).

paramagnetic scattering observed for β-Mn at low temperature is ascribed to zero-point fluctuations $\langle S_L^2 \rangle_{ZP}$. The fluctuations have the characteristic energy $\Gamma = 20$ meV, much larger than the thermal energy but far below the Fermi energy typical for a normal Fermi gas, pointing to the quantum origin. In this sense, the ground state of pure β-Mn may be called 'a quantum spin liquid' with dynamical fluctuations, although in the magnetic excitation spectrum there is no indication of a gap expected for the quantum spin liquid in the general sense [6]. With increasing temperature, we expect an increase of the thermal fluctuations $\langle S_L^2 \rangle_{TH}$, which will be discussed below. For β-$Mn_{0.9}Al_{0.1}$, spin fluctuations are more static or of thermal origin, i.e. $\langle S_L^2 \rangle_{ST}$ or $\langle S_L^2 \rangle_{TH}$. The frequencies of the fluctuations decrease with decreasing temperature, resulting in a narrowing of the energy spectrum, which gives rise to spin-glass-like freezing. Due to the narrow energy window used in the experiment, the slowing down of spin fluctuations leads to a marked increase of the magnetic scattering in the quasi-elastic spectrum. We did not find an appreciable difference in the $\boldsymbol{Q}$-spectra at 7 K (below T_f) and 60 K (above T_f), indicating that the spatial spin correlation does not change markedly at these temperatures on the timescale of neutron scattering. This implies that strong short-range correlations of antiferromagnetic type persist even in the spin-glass-like state. It is worth noting that similar behaviour was found for $Y(Mn_{0.9}Al_{0.1})_2$ [54], indicating the same mechanism for spin freezing for the two systems.

It is of interest to estimate the absolute value of the spin fluctuations. In principle, this is possible by comparing the scattering intensity with that of a certain nuclear Bragg peak. In order to obtain the total amplitude, however, it is necessary to integrate the scattering intensity over both momentum and energy spaces. If the energy resolution is wider than the highest energy of the spin fluctuations, the integration of the quasi-elastic $\boldsymbol{Q}$-spectrum over the whole Brillouin zone gives a full-moment value as follows:

$$\langle S_L^2 \rangle = \int_{BZ} \int_{-\infty}^{+\infty} S(\boldsymbol{q}, \omega)\ \mathrm{d}\omega\ \mathrm{d}\boldsymbol{q} = \int_{BZ} \langle S(\boldsymbol{q})^2 \rangle\ \mathrm{d}\boldsymbol{q} \tag{9}$$

where $\langle S(\boldsymbol{q})^2 \rangle$ is the mean square amplitude of spin fluctuations with the wave vector $\boldsymbol{q}$. Our experimental energy resolution is apparently smaller than the characteristic energy of

Table 1. The energy widths of the scattering functions and the amplitudes of local spin fluctuations.

	T (K)	2Γ (meV)	$\langle M_L\rangle$ (μ_B), ± 3 meV	$\langle M_L\rangle$ (μ_B), ± 10 meV	$\langle M_L\rangle$ (μ_B), ± 30 meV	$\langle M_L\rangle_{TH}$ (μ_B), -30 to 0 meV
β-Mn	7	40 ± 10	—	0.5 ± 0.1	1.0	0.1
	290	60 ± 15	—	0.9 ± 0.1	1.5	1.3
β-$Mn_{0.9}Al_{0.1}$	7	1.3 ± 0.2	1.24 ± 0.05	—		
	60	4.5 ± 0.5	1.03 ± 0.05	—		
	290	20 ± 5	0.60 ± 0.05	0.8 ± 0.1		

spin fluctuations, especially for pure β-Mn. Tentatively, however, following the discussion given by Ziebeck and Brown [36], we have estimated moment values by integrating only the amplitude within the experimental energy resolutions. In order to estimate the absolute value, we compared the scattering amplitude with that of the (221)/(300) nuclear Bragg peak measured in the same experimental conditions, and used the form factor of Mn^{2+} [55]. Here, we assumed that the magnetic scattering observed in the experiments originates only in site II, and that Al atoms occupy only site II. (In reference [34], we assumed that all Mn atoms are responsible for the magnetic scattering.) The values of $\langle M_L\rangle \equiv 2\sqrt{\langle S_L^2\rangle}$ obtained are listed in table 1. For β-Mn, since the energy window $2\Gamma_{res} = 19.3$ meV is much smaller than the characteristic energy of the fluctuations, the values obtained should be much smaller than the full values, but they are already of the order of 1 μ_B even at 7 K, indicating the presence of giant spin fluctuations. It is interesting to compare the absolute values for β-Mn with those for $Y_{0.97}Sc_{0.03}Mn_2$ for which the magnetic scattering was measured by using a spectrometer with the wider energy window $2\Gamma_{res} = 56$ meV installed at the ILL [13]. For this purpose, assuming equation (6) as the energy dependence of $\chi''(\boldsymbol{q}, \omega)$ for extrapolating the energy spectra to $\hbar\omega = \pm 30$ meV, and assuming the q-independence of the energy spectral profile, we calculated moment values within the energy transfer of ± 30 meV, although this is not yet wide enough to cover higher-energy fluctuations. The results are also shown in table 1. These values are a little smaller than those of $Y_{0.97}Sc_{0.03}Mn_2$ (1.3, 1.6, and 1.8 μ_B at 8, 120, and 330 K, respectively [13]). This may be related to the characteristic energies for β-Mn being larger than those for $Y_{0.97}Sc_{0.03}Mn_2$ ($\Gamma \approx 10$ meV at 8 K, $\Gamma \approx 15$ meV at 120 and 330 K), suggesting almost the same magnitude for the fully integrated moment. Here, we want to stress the marked similarity of the overall nature of the spin fluctuations for β-Mn and that for $Y_{0.97}Sc_{0.03}Mn_2$, e.g. the spatial correlations, characteristic energy, temperature dependence, and also the magnitude. For β-$Mn_{0.9}Al_{0.1}$, the moment value at 7 K integrated within $2\Gamma_{res} = 5.8$ meV can be considered as the averaged magnitude of ordered moments $2\sqrt{\langle S_L^2\rangle_{ST}}$, since the spins are almost static. The ordered moment thus estimated for β-$Mn_{0.9}Al_{0.1}$ is 1.24 μ_B, which is in excellent agreement with that estimated from the NMR: $\sim$1.2 μ_B (figure 20), which is local information on site II. This good correspondence justifies the assumption that only site II is responsible for the magnetism. This ordered moment is several times larger than the effective paramagnetic moment estimated from the susceptibility (see figure 4), reflecting a strong $\boldsymbol{Q}$-dependence of the spin-fluctuation spectrum. With increasing temperature, the moment value integrated within $2\Gamma_{res} = 5.8$ meV is reduced. This can be mainly ascribed to the increase of high-energy fluctuations beyond the energy window, resulting in the decrease of amplitude in the quasi-elastic condition. Actually, the moment value at 290 K integrated within $2\Gamma_{res} = 19.3$ meV (figure 19) is nearly the same as that of β-Mn, suggesting that

the temperature dependence of local spin fluctuations, i.e. $\langle S_L^2\rangle_{TH} + \langle S_L^2\rangle_{ST}$, is small for β-$Mn_{0.9}Al_{0.1}$.

It is of interest to extract the thermal part of the spin fluctuations from the total spectrum. It is likely, however, that a unique expression for the thermal moment has not been derived. Ishikawa [56] suggested that only the neutron energy-gain part ($\omega < 0$) of the spectrum gives thermal fluctuations. Although this procedure may be controversial, it may be convenient for the crude estimation of the thermal component in a quantum spin liquid. In this manner we estimated thermal moments $\langle M_L\rangle_{TH}$ for β-Mn, which are listed in table 1. Although there are only two values for different temperatures, we anticipate that the thermal fluctuations $\langle S_L^2\rangle_{TH}$ increase rapidly with increasing temperature, associated with thermal excitations of low-energy spin fluctuations as in the case of $Y_{0.97}Sc_{0.03}Mn_2$ [13].

The nuclear spin–lattice relaxation rate $1/T_1$ is generally given by the dynamical susceptibility as [57]

$$\frac{1}{T_1} = 2\gamma_n^2 k_B T A_{hf}^2 \sum_q \frac{\chi''(q,\omega_n)}{\omega_n} \tag{10}$$

where ω_n is the resonance frequency, and A_{hf} is the hyperfine coupling constant which is assumed to be isotropic. Assuming equation (6) for the dynamical susceptibility, and assuming q-independence of the energy spectrum, and noting that $\hbar\omega_n \ll \Gamma$, equation (10) is reduced to

$$\frac{1}{T_1} = 2\gamma_n^2 k_B T A_{hf}^2 \sum_q \frac{\chi(q)}{\Gamma}. \tag{11}$$

The temperature dependences of both $\chi(q)$ and Γ are responsible for that of $1/T_1$. For localized-moment systems, $\chi(q)$ shows rather weak q-dependence, and obeys the Curie–Weiss law. In this case, $T\chi(q)$ is nearly constant far above the magnetic ordering temperature, and hence Γ determines the temperature dependence of $1/T_1$. When the local spins S interact with each other via the exchange interaction J, Γ ($\sim JS$) does not depend on temperature, leading to a temperature-independent $1/T_1$ at sufficiently high temperatures [57]. At around the critical temperature for the magnetic ordering, on the other hand, it is expected that $\chi(Q)$ diverges, where $\boldsymbol{Q}$ is the propagation vector, and furthermore Γ approaches zero via the critical slowing down of spin fluctuations, giving rise to a divergence of $1/T_1$ at the transition temperature. This was just observed for β-$Mn_{0.9}Al_{0.1}$; nearly temperature-independent behaviour of $1/T_1$ above 100 K indicates the existence of local moments, and the critical increase of the relaxation rate may be explained by the critical slowing down of spin fluctuations just above the freezing temperature of about 50 K. For β-$Mn_{0.97}Al_{0.03}$ we observed a $\sqrt{T}$-dependence of $1/T_1$ at low temperatures, and a trend towards saturation above 50 K. The $\sqrt{T}$-dependence of $1/T_1$ is generally considered to be evidence of antiferromagnetic spin fluctuations, as derived from the SCR theory of spin fluctuations [58, 59]. Thus the result for β-$Mn_{0.97}Al_{0.03}$ indicates antiferromagnetic correlations of spin fluctuations, and the saturation of the amplitude of longitudinal fluctuations at high temperatures. The relaxation rate $1/T_1$ measured for pure β-Mn showed the $\sqrt{T}$-dependence over the entire range of measurements [4, 45]. This implies that in β-$Mn_{0.97}Al_{0.03}$ the large paramagnetic moment is more rapidly induced with increasing temperature, and almost saturates at higher temperatures, indicating that the substitution of Al adds a localized-moment nature to spin fluctuations. Similar behaviour has also been observed in high-pressure-synthesized hexagonal YMn_2 [60] and $YbMn_2$ [61], which do not show magnetic ordering down to low temperatures. From a different point of view, let us consider the relaxation in a quantum spin liquid which condenses to the

singlet ground state. Since neither the divergence of $\chi(Q)$ nor the critical slowing down to 0 K is expected, $1/T_1$ should approach zero at 0 K due to the reduction of the low-energy excitations. At high temperature, however, it may behave as a local moment system, which yields a temperature-independent $1/T_1$. This is the case for β-$Mn_{0.97}Al_{0.03}$. Thus the relaxation behaviours of β-$Mn_{0.97}Al_{0.03}$ and β-$Mn_{0.9}Al_{0.1}$ also support the picture: the transition from a quantum spin liquid to a spin glass caused by the substitution of Al.

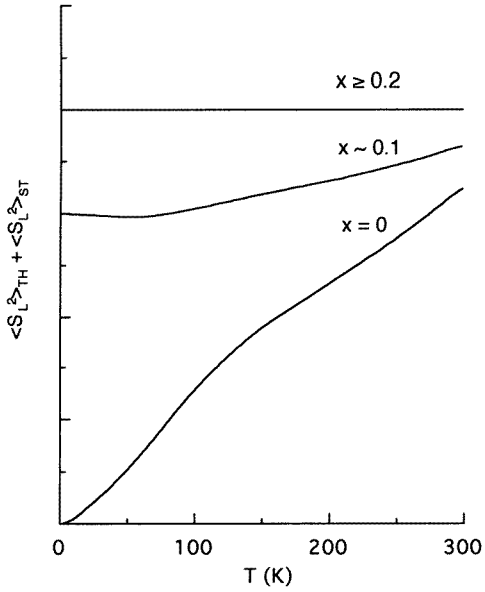

Figure 21. A schematic diagram of the evolution of the thermal and static spin fluctuations $\langle S_L^2\rangle_{TH} + \langle S_L^2\rangle_{ST}$ instigated by the substitution of Al.

The characteristic features of the susceptibility, specific heat, thermal expansion, and electrical resistivity can also be explained in the same context as in reference [19]. We assume that only thermal fluctuations $\langle S_L^2\rangle_{TH}$ and the static spin $\langle S_L^2\rangle_{ST}$ contribute to these properties, and that the temperature dependence varies as in figure 21 against the Al content x. It is assumed that the magnetic entropy S_m originates only from $\langle S_L^2\rangle_{TH}$. The large low-temperature specific heat for β-Mn can be ascribed to the rapid increase of S_m, which should approach $k_B \ln(2S+1)$ at the high-temperature limit, where S is the full spin expected from d-electron occupation. On increasing the Al content x, the static spin $\langle S_L^2\rangle_{ST}$ is induced, and this leads to a reduction of S_m, which leads to a rapid reduction of the γ-value. It is generally accepted that the spontaneous volume magnetostriction is proportional to the squared amplitude of the local spin, i.e. $\langle S_L^2\rangle_{TH} + \langle S_L^2\rangle_{ST}$. The enhanced thermal expansion coefficient for β-Mn can be ascribed to the rapid increase in $\langle S_L^2\rangle_{TH}$ with temperature. The volume expansion observed at low temperatures for $x \sim 0.1$ can be explained by the increase of $\langle S_L^2\rangle_{ST}$. The absence of the thermal expansion anomaly, and a small (normal) expansion coefficient for larger x may be understood as the results of the stabilization of the Mn moment. The temperature dependence of the resistivity can also be interpreted in the same context. The rapid rise at low temperatures for β-Mn can be ascribed to a rapid increase of the collision rate caused by thermal spin fluctuations. At high temperatures, thermal fluctuations saturate to the upper limit value, and hence so does the resistivity.

If $\langle S_L^2\rangle_{TH}$ and $\langle S_L^2\rangle_{ST}$ contribute to electron scattering with the same cross section, it is reasonable that the magnetic resistivity becomes nearly constant for $x \geqslant 0.1$. The existence of strong antiferromagnetic correlations implies Curie–Weiss-like behaviour in the staggered susceptibility $\chi(Q)$ but not in the uniform susceptibility $\chi(0)$, which is the case for β-Mn. With increasing Al content x, localized-moment characteristics appear, leading to an increase in $\chi(0)$.

7.2. Possible frustration in β-Mn

Noting the marked similarity of the Y(Sc)$(Mn_{1-x}Al_x)_2$ and β-$Mn_{1-x}Al_x$ systems in many respects, the suppression of magnetic ordering (the formation of the quantum spin-liquid state), and the dramatic change of the magnetism caused by the Al substitution should be interpreted in the same context as discussed in reference [19], where the physical properties of the Y(Sc)$(Mn_{1-x}Al_x)_2$ system were explained in terms of magnetic frustration on the cubic Laves phase structure. Geometrical frustration of antiferromagnetic interactions has been investigated in detail for low-dimensional lattices such as the two-dimensional triangular lattice and the Kagomé lattice, which are frustrated systems in the sense that they have a macroscopic number of ground-state degeneracies. The Kagomé lattice, i.e. a network of *corner-sharing* regular triangles, is more *highly* frustrated due to the small coordination number. In three-dimensional systems, it is known that antiferromagnetic spins frustrate on a regular tetrahedron and its network. An example is found in the fcc lattice, which is a network of edge-sharing tetrahedra. Another example is the network of *corner-sharing* tetrahedra found in pyrochlore, the spinel lattice, and the Laves phase. Frustration on the corner-sharing tetrahedra was first discussed theoretically by Anderson [23] for Ising spins and by Villain [24], and recently in more detail by Reimers *et al* [25, 26] for Heisenberg spins. From an experimental point of view the corner-sharing tetrahedral lattice is much more interesting, since it is *highly* frustrated and there is no great degree of interaction between second-nearest and further neighbours, in contrast with the case for most fcc compounds. The equivalence of the Mn site in C15-type Y(Sc)Mn_2 to the tetrahedral network led us to the interpretation of the magnetic properties for the Y(Sc)$(Mn_{1-x}Al_x)_2$ system in terms of frustration.

Table 2. Atomic positions of the β-Mn (A13) structure.

Site I	x, x, x	$3/4-x, 3/4-x, 3/4-x$	$1/2+x, 1/2-x, -x$
	$1/4-x, 3/4+x, 1/4+x$	$-x, 1/2+x, 1/2-x$	$1/4+x, 1/4-x, 3/4+x$
	$1/2-x, -x, 1/2+x$	$3/4+x, 1/4+x, 1/4-x$	
Site II	$1/8, y, 1/4+y$	$3/8, -y, 3/4+y$	$7/8, 1/2+y, 1/4-y$
	$5/8, 1/2-y, 3/4-y$	$1/4+y, 1/8, y$	$3/4+y, 3/8, -y$
	$1/4-y, 7/8, 1/2+y$	$3/4-y, 5/8, 1/2-y$	$y, 1/4+y, 1/8$
	$-y, 3/4+y, 3/8$	$1/2+y, 1/4-y, 7/8$	$1/2-y, 3/4-y, 5/8$

There have not, to the best of our knowledge, been any theoretical arguments on geometrical frustration on the β-Mn (A13) structure. Here, we briefly discuss the possibility of geometrical frustration on the β-Mn lattice. The positions of site-I and site-II atoms in the unit cell are tabulated in table 2. Experimentally obtained parameters x and y have been reported by different authors: $x = 0.061$ and $y = 0.206$ in an earlier study by Preston [38], and $x = 0.0636$ and $y = 0.2022$ from a more precise analysis by Shoemaker *et al* [62]. It has generally been accepted that the structure of β-Mn is difficult to describe, as

Table 3. Neighbouring distances for a site-II atom when $y = 0.2022$. (Only site-II atoms are considered.)

	Number of neighbours	Distances*
1	4	0.4190
2	2	0.4233
3	2	0.5180

*In units of the lattice parameter.

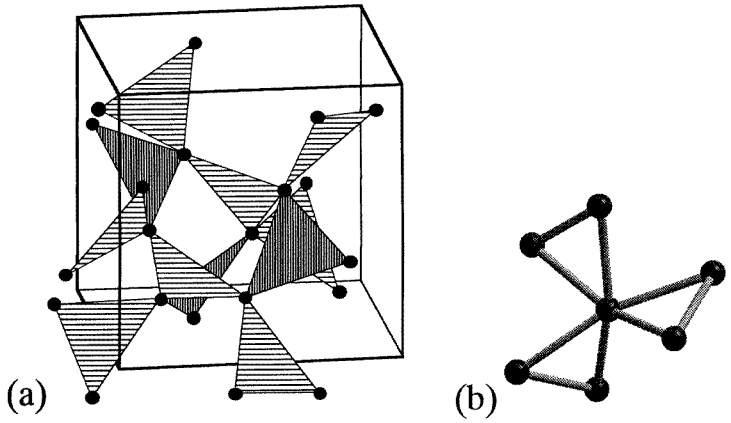

Figure 22. (a) A schematic diagram of the site-II sublattice in the β-Mn-type structure, which is a network of corner-sharing regular triangles. All triangle planes are normal to one of the $\langle 111 \rangle$ axes. In general, the size of the triangle A (vertically hatched) is slightly different from that of B (horizontally hatched) but becomes identical in the case where $y = (9-\sqrt{33})/16 = 0.203\,46\ldots$ (see the text). (b) A 'distorted windmill' element made up of three corner-sharing regular triangles. The angle ϕ between two triangles satisfies $\cos\phi = 1/3$ or $-1/3$.

conjectured on the basis of figure 1. Some efforts to describe the characteristic atomic arrangements have been made—for example, icosahedral packing sequences formed by all of the atoms on both sites I and II discussed by Kripyakevich [63], and an elegant description in terms of body-centred cubic rod packing by O'Keeffe and Andersson [64] (see also recent work by Nyman *et al* [65] and O'Keeffe [66]). However, here, we propose a new description concerning the frustration; we consider only site II, since only this site seems to be *magnetic* and not magnetically coupled with the other site as discussed in a previous section. Although this independent treatment of the same Mn atoms may appear strange, and we cannot exclude the possibility of weak magnetism of the site-I atoms, this assumption considerably simplifies the argument, as follows. The neighbouring distances, obtained taking into account only site II and assuming $y = 0.2022$ (the value reported by Shoemaker *et al*), are listed in table 3. It is notable that the nearest-neighbour (NN) and next-nearest-neighbour (NNN) distances are very close, and considerably smaller than third- and further-neighbour distances. If we confine our attention to the bonds between only NN and NNN atoms, the site-II sublattice is characterized by a network of corner-sharing regular triangles, as shown in figure 22(a). Each site-II atom bonds with six neighbouring site-II atoms, as three triangles share those corners. It should be noted that each triangle plane is normal to one of the four different $\langle 111 \rangle$ axes, and that the angle ϕ between two triangles satisfies $\cos\phi = 1/3$ or $-1/3$. Hence a triangle plane is twisted from the others like a

'distorted windmill', as shown in figure 22(b), where only an element made up of three triangles is shown. In general, the size of a triangle, say A, is slightly different from that of the other two triangles B. It should be noted, however, that NN and NNN interatomic distances become identical in the case where

$$y = \frac{9 - \sqrt{33}}{16} = 0.203\,46\ldots$$

as was already pointed out by O'Keeffe and Andersson [64]. (In this case the NN interatomic distance is $0.420\,17\,a$.) In fact, the reported values of y are very close to this ideal value. The value $y = 0.206$ reported by Preston gives the triangle A as larger than B, while $y = 0.2022$ reported by Shoemaker *et al* gives the opposite result. This suggests that NN and NNN distances can to a great extent be seen as the same within experimental accuracies. In fact, we even believe that those distances should be the same for higher symmetry. It should also be noted that the interaction with further neighbours should be small, as in the case of the corner-sharing tetrahedral lattice. In this case, this lattice is reminiscent in some respects of the two-dimensional Kagomé lattice, which is also a network of corner-sharing regular triangles but in which two triangles share those corners. Then this lattice may be called a 'three-dimensional Kagomé lattice', which may be an interesting topic for a theoretical study. This lattice should be compared with similar three-dimensional magnetic sublattices made up of corner-sharing triangles found in gadolinium gallium garnet (GGG), in which two triangles share those corners [67, 68]. The two-dimensional Kagomé lattice, and also its three-dimensional analogue, the corner-sharing tetrahedral lattice, have already been investigated extensively, and effects of frustration have been argued for Heisenberg spins [6, 24–26]. Assuming only NN exchange, a q-independent spin-wave branch throughout the whole zone, i.e. no long-range order, has been predicted for both lattices within the mean-field approximation [25]. This argument may be valid for the β-Mn lattice as a network of corner-sharing triangles. Recently, Asada [69] suggested the frustration of the antiferromagnetic interaction on site II in β-Mn. According to his calculation, taking into account only 12 site-II atoms in the crystallographic unit cell, there are 26 inequivalent spin alignments with the lowest total energy. Although there have not been precise arguments for the infinite lattice, we may expect the macroscopic number of degeneracies of ground states for this lattice, and some effects of frustration on the physical properties of β-Mn. Thus, naively, it is clear that the effects of frustration are critical in discussing the magnetism of β-Mn. However one may expect coupling beyond nearest neighbours. We speculate that NN coupling, at least, in β-Mn is strong enough for frustration to determine the essential nature of the magnetism. However, arguments for insulators are apparently irrelevant as regards certain details. For highly frustrated insulators, some kinds of transition have been found at very low temperatures, and random dilution leads to unconventional behaviour in addition to conventional spin-glass ordering (see [7], and references cited therein). These observations have also been justified by some theoretical work [70–78]. The reason for the situation in the β-Mn system being different from that for insulators lies mainly in the fact that β-Mn is classified as an itinerant magnet located in the magnetic–non-magnetic instability region. The effects of frustration in the itinerant system have already been examined extensively for the RMn_2 system [8–11]. In the system, it has been suggested that short-wavelength spin-density fluctuations are enhanced by the frustration, and the formation of a local spin singlet is favoured. Recently, Ballou *et al* [18] performed precise neutron scattering measurements of single-crystalline $Y(Sc)Mn_2$, and demonstrated the presence of short-lived four-site collective spin singlets, which are inherent to the network of tetrahedra. We consider that the nature of β-Mn should be

discussed on the basis of the same context; β-Mn is characterized by enhanced effects of frustration in the vicinity of the magnetic–non-magnetic instability, and the quantum spin-liquid state—presumably a certain local spin-singlet state—is favoured only for the perfect lattice. Spin-glass-like behaviour induced by the Al substitution should relate to not only the release of frustration but also the stabilization of on-site local moments (instability of the local spin-singlet state) associated with lattice volume expansion (i.e. decrease of the bandwidth), and the introduction of randomness. This idea may explain why the spin-glass-like ground states appear at Al concentrations much smaller than that expected from simple percolation considerations. Thus we suppose that the validity of theories for insulators is limited for these itinerant systems, especially as regards discussion of the ground-state selection and properties at very low temperatures. New theoretical approaches dealing with frustration in itinerant systems seem to be necessary. Experimentally, since our results are limited to 1.4 K, measurements at lower temperatures will be interesting. It is also of great interest to observe the more detailed structure of the dynamical susceptibility for β-Mn, so as to reveal the real ground state and spin dynamics in the network of triangles.

8. Conclusions

We have systematically investigated the magnetic properties of the β-$Mn_{1-x}Al_x$ system ($0 \leqslant x \leqslant 0.4$). A quantum spin-liquid state with strong antiferromagnetic correlations was revealed in β-Mn. The substitution of Al atoms, which occupy site II, converts the ground state to one of spin-glass type. The origin of these characteristics was discussed in terms of geometrical frustration on site II in the β-Mn (A13) structure, which is a network of corner-sharing regular triangles twisted with respect to each other. Hence the magnetism of β-Mn is reduced to that of an infinite network of corner-sharing triangles, which is in some respects identical to the two-dimensional Kagomé lattice. Our scenario is as follows: the ground state of pure β-Mn can be regarded as a quantum spin liquid, which is possibly realized as a result of frustration of the antiferromagnetic interactions, and non-magnetic impurity releases the spin-configurational degeneracies originating in the frustration, and gives rise to a spin-glass-like state.

As well as Mn-based Laves phase compounds, the present study of β-Mn gives another example in metallic magnets in which frustration plays a leading role in determining the magnetic properties. Finally, it should be emphasized that β-Mn is not a 'weak' magnet, but, even at the lowest temperature, is a rather strong magnet with a large dynamical moment. Furthermore, β-Mn is the most ideally homogeneous system in which a magnetically disordered ground state has been found.

Acknowledgments

The authors are indebted to Dr H Wada for collaboration in some parts of this study, and to Professor M Mekata, Professor K Motoya, and Professor T Asada for helpful discussion. They are also grateful for Messrs T Suzuki, T Yaegashi, and N Asai for assistance in the neutron diffraction measurements, and to Mr R Iehara for much technical support. This work was partially supported by a Grant-in-Aid for Scientific Research given by the Ministry of Education, Science and Culture of Japan.

References

[1] Kasper J S and Roberts B W 1956 *Phys. Rev.* **101** 537
[2] Masuda Y, Asayama K, Kobayashi S and Itoh J 1964 *J. Phys. Soc. Japan* **19** 460
[3] Shinkoda T, Kumagai K and Asayama K 1979 *J. Phys. Soc. Japan* **46** 1754
[4] Katayama M, Akimoto S and Asayama K 1977 *J. Phys. Soc. Japan* **42** 97
[5] Liebmann R 1986 *Statistical Mechanics of Periodic Frustrated Ising Systems* (Berlin: Springer)
[6] Chandra P and Coleman P 1995 *Strongly Interacting Fermions and High T_c Superconductivity* ed B Doucot and J Zinn-Justin (Amsterdam: North-Holland) p 495
[7] Ramirez A P 1994 *Annu. Rev. Mater. Sci.* **24** 453
[8] See, for example,
Shiga M 1994 *J. Magn. Magn. Mater.* **129** 17
[9] Ballou R, Lacroix C and Nunez Reguerio M D 1991 *Phys. Rev. Lett.* **66** 1910
[10] Nunez Reguerio M D and Lacroix C 1994 *Phys. Rev.* B **50** 16 063
[11] Pinettes C and Lacroix C 1994 *J. Phys.: Condens. Matter* **6** 10 093
[12] Nakamura H, Wada H, Yoshimura K, Shiga M, Nakamura Y, Sakurai J and Komura Y 1988 *J. Phys. F: Met. Phys.* **18** 981
[13] Shiga M, Wada H, Nakamura Y, Deportes J, Ouladdiaf B and Ziebeck K R A 1988 *J. Phys. Soc. Japan* **57** 3141
[14] Shiga M, Wada H, Nakamura Y, Deportes J and Ziebeck K R A 1988 *J. Physique Coll.* **49** C8 241
[15] Yoshimura K, Nakamura H, Takigawa M, Yasuoka H, Shiga M and Nakamura Y 1987 *J. Magn. Magn. Mater.* **70** 142
[16] Nakamura H, Kitaoka Y, Yoshimura K, Kohori Y, Asayama K, Shiga M and Nakamura Y 1988 *J. Physique Coll.* **49** C8 257
[17] Wada H, Shiga M and Nakamura Y 1989 *Physica* B **161** 197
[18] Ballou R, Lelièvre-Berna E and Fåk B 1996 *Phys. Rev. Lett.* **76** 2125
[19] Shiga M, Fujisawa K and Wada H 1993 *J. Phys. Soc. Japan* **62** 1329
[20] Mekata M, Asano T, Sugino T, Nakamura H, Asai N, Shiga M, Keren A, Kojima K, Luke G M, Luke W D, Wu W D, Uemura Y J, Dunsinger S and Gingras M 1995 *J. Magn. Magn. Mater.* **140–144** 1767
[21] Shiga M 1995 *Proc. 30th Zakopane School of Physics (Krakow, 1995)* (Singapore: World Scientific) p 57
[22] Nakamura H, Takayanagi F, Shiga M, Nishi M and Kakurai K 1996 *J. Phys. Soc. Japan* **65** 2779
[23] Anderson P W 1956 *Phys. Rev.* **102** 1008
[24] Villain J 1979 *Z. Phys.* B **33** 31
[25] Reimers J N, Berlinsky A J and Shi A-C 1991 *Phys. Rev.* B **43** 865
[26] Reimers J N 1992 *Phys. Rev.* B **45** 7287
[27] Kohara T and Asayama K 1974 *J. Phys. Soc. Japan* **37** 37
[28] Mekata M, Nakahashi Y and Yamaoka T 1974 *J. Phys. Soc. Japan* **37** 1509
[29] Hori T 1975 *J. Phys. Soc. Japan* **38** 1780
[30] Akimoto S, Kohara T and Asayama K 1975 *Solid State Commun.* **16** 1227
[31] Nishihara Y, Ogawa S and Waki S 1977 *J. Phys. Soc. Japan* **42** 845
[32] Katayama M and Asayama K 1978 *J. Phys. Soc. Japan* **44** 425
[33] Shiga M, Yoshimoto K, Nakamura H and Wada H 1993 *Int. J. Mod. Phys.* **7** 1008
[34] Shiga M, Nakamura H, Nishi M and Kakurai K 1994 *J. Phys. Soc. Japan* **63** 1656
[35] Shiga M, Nakamura H, Nishi M and Kakurai K 1995 *J. Magn. Magn. Mater.* **140–144** 2009
[36] Ziebeck K R A and Brown P J 1980 *J. Phys. F: Met. Phys.* **10** 2015
[37] Dorner B 1982 *Coherent Inelastic Neutron Scattering in Lattice Dynamics* (Berlin: Springer) p 13
[38] Preston G D 1928 *Phil. Mag.* **5** 1207
[39] Izumi F, Asano H, Murata H and Watanabe N 1987 *J. Appl. Crystallogr.* **26** 411
[40] Oyamatsu H, Nakai Y and Kunitomi N 1989 *J. Phys. Soc. Japan* **58** 3606
[41] Mori N, Ukai T and Sasaki K 1981 *Physics of Transition Metals 1980 (Inst. Phys. Conf. Ser. 55)* ed P Rhodes (Bristol: Institute of Physics Publishing) p 21
[42] Whittaker K C, Dziwornooh P A and Riggs R J 1971 *J. Low Temp. Phys.* **5** 461
[43] Hauser R, Bauer E, Gratz E, Dubenko I S and Markosyan A S 1994 *Physica* B **199+200** 662
[44] Drain L E 1966 *Proc. Phys. Soc.* **88** 111
[45] Kohori Y, Noguchi Y and Kohara T 1993 *J. Phys. Soc. Japan* **62** 447
[46] See, for example,
Das T P and Hahn E L 1958 *Solid State Physics* Suppl. 1, ed F Seitz and D Turnbull (New York: Academic) p 14

[47] Narath A 1967 *Phys. Rev.* **162** 320
[48] Funahashi S and Kohara T 1984 *J. Appl. Phys.* **55** 2048
[49] El-Hannany U and Warren W W Jr 1975 *Phys. Rev.* B **12** 861
[50] Yamada T, Kunitomi N, Nakai Y, Cox D E and Shirane G 1970 *J. Phys. Soc. Japan* **28** 615
[51] Yamagata H and Asayama K 1970 *J. Phys. Soc. Japan* **29** 1385
[52] Takahashi Y 1990 *J. Phys.: Condens. Matter* **2** 8405
[53] Takahashi Y 1986 *J. Phys. Soc. Japan* **55** 3553
[54] Motoya K, Freltoft T, Böni P and Shirane G 1988 *Phys. Rev.* **38** 4796
[55] Watson R E and Freeman A J 1961 *Acta Crystallogr.* **14** 231
[56] Ishikawa Y 1983 *J. Magn. Magn. Mater.* **31–34** 309
[57] Moriya T 1956 *Prog. Theor. Phys. (Kyoto)* **16** 641
[58] Moriya T and Ueda K 1974 *Solid State Commun.* **15** 169
[59] Ueda K and Moriya T 1975 *J. Phys. Soc. Japan* **38** 32
[60] Nakamura H, Moriwaki M, Shiga M, Inoue K, Nakamura Y, Tsvyashchenko A and Fomicheva L 1995 *J. Magn. Magn. Mater.* **140–144** 803
[61] Nakamura H, Moriwaki M, Shiga M, Inoue K, Nakamura Y, Tsvyashchenko A and Fomicheva L 1997 *J. Magn. Magn. Mater.* at press
[62] Shoemaker C B, Shoemaker D P, Hopkins T E and Yindepit S 1978 *Acta Crystallogr.* B **34** 3573
[63] Kripyakevich P I 1960 *Sov. Phys.–Crystallogr.* **5** 275
[64] O'Keeffe M and Andersson S 1977 *Acta Crystallogr.* A **33** 914
[65] Nyman H, Carroll C E and Hyde B G 1991 *Z. Kristallogr.* **196** 39
[66] O'Keeffe M 1992 *Acta Crystallogr.* A **48** 879
[67] Schiffer P, Ramirez A P, Huse D A and Valentino A J 1994 *Phys. Rev. Lett.* **73** 2500
[68] Schiffer P, Ramirez A P, Huse D A, Gammel P L, Yaron U, Bishop D J and Valentino A J 1995 *Phys. Rev. Lett.* **74** 2379
[69] Asada T 1995 *J. Magn. Magn. Mater.* **140–144** 47
[70] Harris A B, Kallin C and Berlinsky A J 1992 *Phys. Rev.* B **45** 2899
[71] Chalker J T, Holdsworth P C W and Shender E F 1992 *Phys. Rev. Lett.* **68** 855
[72] Singh R R P and Huse D A 1992 *Phys. Rev. Lett.* **68** 1766
[73] Huse D A and Rutenberg A D 1992 *Phys. Rev.* B **45** 7536
[74] Sachdev S 1992 *Phys. Rev.* B **45** 12 377
[75] Chubukov A 1992 *Phys. Rev. Lett.* **69** 832
[76] Chandra P, Coleman P and Ritchey I 1993 *J. Physique* I **3** 591
[77] Kuroda A and Miyashita S 1995 *J. Phys. Soc. Japan* **64** 4509
[78] Shender E F, Cherepanov V B, Holdsworth P C W and Berlinsky A J 1993 *Phys. Rev. Lett.* **70** 3812